Scanning Electron Microscopy

Volume 1982
Number 1 *1982*

Article 13

1982

# Monte Carlo Electron Trajectory Calculations of Electron Interactions in Samples with Special Geometries

Dale E. Newbury
*National Bureau of Standards*

Robert L. Myklebust
*National Bureau of Standards*

Electron Beam Interactions With Solids (Pp. 153-163)
SEM, Inc., AMF O'Hare (Chicago), IL 60666, U.S.A.

# MONTE CARLO ELECTRON TRAJECTORY CALCULATIONS OF ELECTRON INTERACTIONS IN SAMPLES WITH SPECIAL GEOMETRIES

Dale E. Newbury* and Robert L. Myklebust

National Bureau of Standards
Washington, DC 20234

## ABSTRACT

Implementing a Monte Carlo simulation for application to electron sample interactions requires use of accurate treatments of elastic and inelastic scattering. In formulating a Monte Carlo simulation, careful testing must be carried out to ensure that the calculation yields sensible and useful results. A suitable testing procedure includes calculation of (1) electron backscatter coefficients as a function of atomic number, including any necessary adjustment of scattering parameters; (2) backscatter coefficients as a function of specimen tilt; (3) backscatter and transmission coefficients for thin foils; (4) backscattered electron energy distributions; (5) electron spatial distributions; and (6) x-rays, including x-ray depth distributions, and relative and absolute yields.

Adapting a Monte Carlo simulation to a particular problem involving special sample geometry requires careful consideration of the interaction of the electron with the target. When the electron trajectory crosses a boundary, the segments of the trajectory in each phase must be calculated in a logical, stepwise fashion, allowing for modification of the step lengths due to variable scattering power in phases of different composition. The particular example of a planar boundary between phases of different composition is considered.

**Keywords:** (1) electron probe microanalysis; (2) electron scattering; (3) electron-specimen interactions; (4) Monte Carlo electron trajectory simulation; (5) scanning electron microscopy; (6) x-ray microanalysis.

*Address for correspondence:
A121/222
N.B.S.
Washington, DC 20234
Phone No. (301) 921-2875

## INTRODUCTION

Monte Carlo electron trajectory simulation techniques have proven to be of great utility in the study of electron-sample interactions in scanning electron microscopy, electron probe x-ray microanalysis, electron beam lithography, and analytical electron microscopy (Heinrich et al., 1976; Shimizu and Murata, 1971; Kyser, 1981; Newbury and Myklebust, 1981). The Monte Carlo technique involves a step-wise simulation of the electron trajectory in the target. Scattering angles and mean free paths are calculated from appropriate equations for elastic and inelastic scattering. A number of distinct variations on the implementation of the Monte Carlo technique for solid specimens have been described, including discrete "single" elastic scattering, "multiple" elastic scattering, continuous energy loss for inelastic scattering, and discrete inelastic scattering. The basic principles of the Monte Carlo technique and the various approaches to combining the scattering models have been recently reviewed (Kyser, 1981). It is possible for interested readers to construct a Monte Carlo simulation for application to their problems based on the descriptions available in the literature. Two topics which should be addressed for the successful development of a useful Monte Carlo simulation and which are not generally discussed in the literature are (1) procedures for testing the Monte Carlo simulation to ensure that the calculation is producing reliable results and (2) adapting the simulation to the particular geometry of a target of interest. In this paper we shall describe the procedures which we employ in developing and testing Monte Carlo electron trajectory simulations for conventional bulk targets as well as targets with special geometries.

## PROCEDURES FOR TESTING MONTE CARLO SIMULATIONS

### A. Adjustable parameters

Several of the Monte Carlo procedures which have been described in the literature make use of an adjustable parameter which is necessary to bring the calculation into agreement with selected experimental data such as backscattering coefficients. In the multiple scattering model of Curgenven and Duncumb (1971), this adjustable parameter took the form of an atomic-number-dependent maximum impact parameter which determined the distribution of scattering

angles. In the single scattering model of Kyser and Murata (1974), a multiplicative factor $(1+(Z/c))$, where Z is the atomic number and c is a constant, was used to modify the mean free path for elastic scattering. The justification for including such modifications to the scattering models is based on the known shortcomings of the simple analytic functions used to describe the scattering models, particularly the screened Rutherford scattering model for elastic scattering. Reimer and Krefting (1976) have shown that the Mott cross section for elastic scattering differs considerably from the Rutherford cross section, particularly for high atomic number targets and low beam energies. Unfortunately, the Mott cross section cannot be expressed in a simple analytic form, and thus it remains a computational advantage to make use of the Rutherford cross section with a modification parameter which can be expressed in the form of a simple equation.

The basic data which we can use to test and adjust the Monte Carlo calculation is the electron backscatter coefficient, $\eta$, defined as

$$\eta = n_{BS} / n$$

where n is the total number of electrons incident upon the sample and $n_{BS}$ is the number of electrons which backscatter as a result of single and multiple scattering. Backscattering coefficients as a function of atomic number have been carefully determined by Bishop (1966) and Heinrich (1966). By calculating $\eta$ as a function of atomic number, Z, with various values for the constant c in the multiplication factor above, a value of $c = 300$ was determined by Kyser and Murata (1974). A comparison of backscatter coefficients calculated with the Rutherford cross section with and without the atomic number dependent modification to the step length is shown in Table I. A full plot of the calculated and measured backscatter coefficients is shown in Figure 1. The correspondence of the calculated backscatter coefficients to experimental values is excellent after adjustment of the step length with the multiplicative factor, whereas without the adjustment the calculated backscatter coefficients were higher by 5 to 10 percent depending on the atomic number.

### B. Backscatter coefficient as a function of tilt and thickness

Having made such a modification to the mean free path, or equivalently to the elastic scattering cross section, in order to achieve agreement with a major interaction characteristic such as the backscattering coefficient, the simulation should be further tested against other measurable characteristics of the interaction. With no further modification to the adjustable parameter(s), satisfactory agreement should be obtained. Suitable data to examine include: (1) the backscatter coefficient as a function of the angle of tilt. An example of the calculated backscatter coefficient as a function of tilt compared to experimental results is shown in Figure 2. (2) Transmission and backscatter coefficients of thin foils. Strictly speaking, backscattering results from a single scattering event through an angle greater than 90 relative to the incident direction so that the electron propagates back through the surface which it initially entered. However, the backscattering coefficient defined above includes all electrons which exit the sample, including both the electrons which backscatter in a single event and those which escape the specimen after undergoing multiple scattering. One way in which the effects of single event backscattering and multiple event backscattering can be separated experimentally is to make use of thin foils in which electron penetration through the foil limits the opportunity for multiple scattering. Single event backscattering will predominate if the foil thickness is of the order of one mean free path as calculated from the total elastic scattering cross section. Thus, by calculating the backscattering coefficient and the transmission coefficient as a function of thickness, the accuracy with which single scattering is modeled can be studied as well as the transition to multiple scattering. An example of such a calculation is shown in Figure 3 for the experimental data of Cosslett and Thomas (1964). Reimer and Krefting (1976) have provided valuable experimental data for thin foils of various elements and thicknesses over a range of beam energies. These calculations on foils of progressively greater thickness also serve to test the capability of the Monte Carlo procedure to estimate the range of the electrons within the solid. The quality of the experimental data on the range is generally poorer than that on backscatter coefficients, due to the slow rate of change of the measured signals near the limit of the range.

### C. Backscatter as a function of energy

Another experimental observation of the behavior of the backscattering coefficient which is useful to test is the response to changes in the beam energy. It is a somewhat surprising experimental observation that the backscatter coefficient does not show a strong trend with beam energy over the range 10-50 keV. An example of the calculated behavior of

### LIST OF SYMBOLS

| | | |
|---|---|---|
| A,B,C | = | direction cosines |
| $A_w$ | = | atomic weight |
| $E_{BS}$ | = | backscattered electron energy |
| $E_c$ | = | critical ionization energy |
| E | = | incident beam energy |
| k | = | the k-value or ratio of x-ray intensity measured on the sample to the standard |
| $N_A$ | = | Avogadro's number |
| $n_{BS}$ | = | number of backscattered electrons |
| $n_T$ | = | number of transmitted electrons |
| n | = | number of incident electrons |
| Q | = | cross section for the process of interest |
| S | = | step length of the calculation with various subscripts |
| X,Y,Z | = | coordinates for Monte Carlo calculations: with various subscripts |
| Z | = | atomic number |
| $\eta$ | = | backscattering coefficient |
| $\theta$ | = | tilt angle |
| $\varrho$ | = | density |
| $\sigma$ | = | standard deviation |
| $\sigma_R$ | = | relative standard deviation |
| $\phi(\varrho z)$ | = | x-ray generation depth distribution function |
| $\omega$ | = | fluorescence yield |

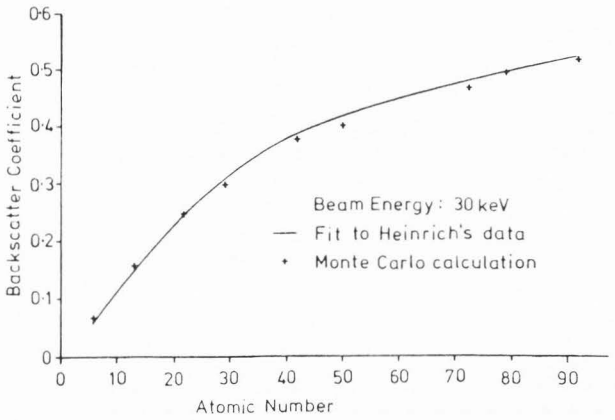


**Fig. 1. Backscatter coefficient as a function of atomic number; Monte Carlo calculations (10,000 trajectories per point); experimental data of Heinrich (1966).**

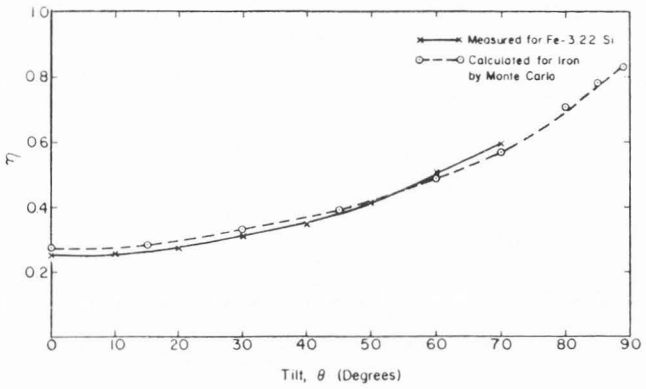


**Fig. 2. Backscatter coefficient as a function of tilt angle $\theta$ for a target of iron. Monte Carlo calculations (10,000 trajectories per point) and experimental data from Myklebust et al. (1976).**

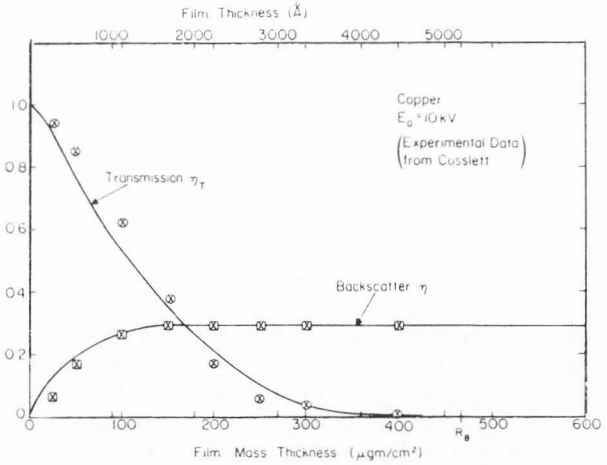


**Fig. 3. Backscatter and transmission coefficients for copper thin foils; Monte Carlo calculations (points, 10000 trajectories) from Myklebust et al (1976); solid lines give a fit to experimental data from Cosslett and Thomas (1966).**

the backscattering coefficient as a function of energy is given in Table 2 along with selected experimental data of Heinrich (1966). A slight trend to lower calculated backscatter coefficients with increasing energy is observed. This trend is opposite to the slight increase in backscattering with increasing energy which is observed experimentally.

It is appropriate at this point to consider the statistical uncertainty associated with a Monte Carlo calculation. Given that the random number generators employed in the calculation are carefully contrived to contain no systematic deviations from randomness, then the effect of repeating a calculation for a given set of beam and specimen parameters is to yield a result with a standard deviation which is given by $\sigma = n_i^{1/2}$ where i refers to the particular signal which is being calculated and $n_i$ is the number of events of that type which occur. Thus although 10000 electron trajectories may be calculated for an aluminum target, the backscattering coefficient at normal incidence is approximately 0.15, which gives a total of 1500 backscattering events. The standard deviation for the calculation of the backscatter coefficient is $1500^{1/2}$ and not $10000^{1/2}$, whereas for a parameter such as the x-ray yield the full number of trajectories contributes to the calculation. To achieve a statistical uncertainty of $\sigma_R$ = one percent relative in the backscatter coefficient in the case of aluminum would require $n = (1/\sigma_R^2) / \eta$ or 66666 trajectories. On the other hand, a calculated parameter to which all of the incident electrons contribute, such as inner shell ionization in the surface layer, will have the benefit of all of the incident electrons in determining the statistics of the calculation. The necessity of calculating even larger numbers of trajectories becomes apparent if a fractional parameter such as the backscatter coefficient is further divided into energy and/or angular distributions.

**Table 1. Backscatter coefficient as a function of atomic number**

Beam energy 20 keV (20000 trajectories)

| Element | Rutherford cross section | $\sigma$ | Rutherford cross section /(1 + (Z/300)) | Heinrich (1966) data |
|---|---|---|---|---|
| Si | .1810 | .002 | .1680 | .164 |
| Ni | .3150 | .004 | .3072 | .301 |
| Au | .5367 | .005 | .5161 | .516 |

**Table 2. Backscatter coefficient versus beam energy**

**Target: gold (20000 trajectories, relative $\sigma_R$ = 1 percent)**

| Energy (keV) | Calculated | Measured (Heinrich, 1966) |
|---|---|---|
| 10 | .5268 | .483 |
| 20 | .5161 | .506 |
| 30 | .4933 | .512 |
| 40 | .4904 | .510 |

### D. Angular distributions

Despite the difficulties noted above, calculation of the angular and energy distributions is of value in testing a Monte Carlo simulation. An example of a distribution partitioned in both energy and scattering angle is shown in Figure 4. In this calculation, the angular distribution of the so-called "low loss electrons", that is, those beam electrons which have lost less than a specified percentage of the incident energy, in this case less than 2.5 percent, has been calculated. The Monte Carlo results (solid line) compare favorably with the experimental results of Wells (1975). In this particular situation, the Monte Carlo calculation can be modified slightly in view of the character of the result to speed up the calculation. Since we are only interested in electrons with energies in the range 19.5-20 keV, the calculation of a given trajectory can be terminated when the energy decreases below 19.5 keV, thus greatly reducing the calculation time.

### E. Energy distributions

To this point all of the test calculations have served principally to examine the simulation of elastic scattering. Inelastic scattering or energy loss is only indirectly tested since energy loss serves to define the maximum length of the electron trajectory. Energy loss thus acts to prevent all beam electrons from eventually undergoing sufficient multiple scattering to reach the surface and backscatter. A good fit to the backscattering process suggests a reasonable treatment of energy loss. A more direct view of the simulation of energy loss can be obtained by calculating the energy distribution of backscattered and/or transmitted electrons. One difficulty in this case is the basis for comparison of calculated results with experimental results. Because of the limited solid angle of collection of electron spectrometers used in the experimental measurements, the experimental energy spectra are determined at a specific take-off angle above the specimen surface and over a small solid angle of perhaps 0.1 steradian. To limit the Monte Carlo calculation to these conditions reduces the number of backscattered electrons to about 1 percent of the total emitted. If this small fraction is further sub-divided into an energy distribution, the statistics of the calculation are unacceptable. We thus tend to use a greater angular range for the energy distribution calculated with the Monte Carlo. An example of the energy distribution for a copper target is shown in Figure 5 in comparison with the experimental energy spectrum of Bishop (1966). Despite the limitations noted, the agreement is reasonably close.

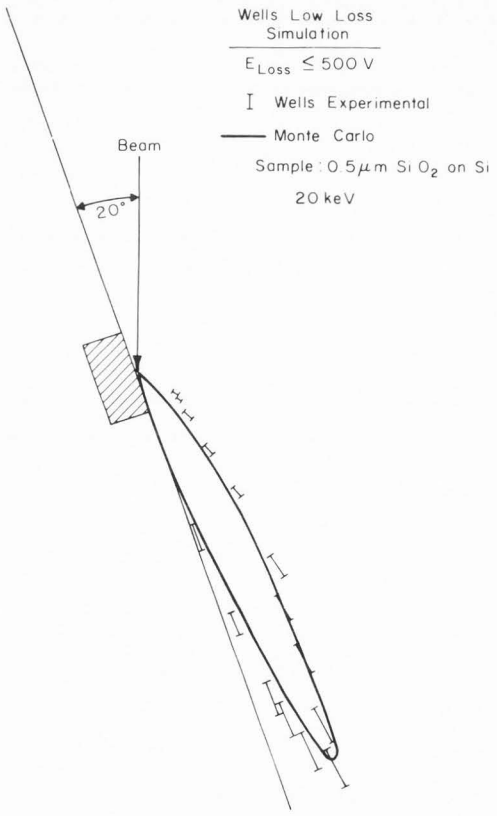


**Fig. 4. Comparison of angular distribution of low-loss backscattered electrons; Monte Carlo electron trajectory calculations from Myklebust et al. (1976); experimental data from Wells (1975).**

### F. Energy deposition

Another experiment which tests the calculation of energy loss is the determination of energy deposition in certain electron-resist materials used in electron beam lithography. These materials, such as polymethylmethacrylate, can be "developed" by etching with suitable solvents to reveal contours of constant energy deposition. The Monte Carlo calculation can then be used to calculate energy deposition in this material for comparison, as illustrated by the results of Shimizu et al. (1975) in Figure 6. This type of calculation not only tests the energy loss calculation, but also the spatial extent of the beam, which is difficult to determine experimentally in opaque, solid materials such as metals.

### G. Spatial distributions

In the process of implementing a calculation, the spatial extent of the interaction volume is often of interest. The interaction volume is often displayed in the form of the familiar computer drawings of the electron trajectories prepared from a sequence of x,y,z coordinates for each trajectory as illustrated in Figures 7(a) and 7(b). While such drawings are useful in a qualitative sense to obtain an impression of the size and shape of the interaction volume, they convey limited quantitative information, and due to the overlap of successive trajectory plots, especially near the beam impact point, it is generally not possible to plot more than about 200 trajectories with sufficient resolution to observe individual trajectories. It is impractical to use plotting to assess the extent of the interaction volume in calculations with a realistic number of trajectories, e.g. 10,000 or more. In this case it is necessary to obtain distribution histograms along the positive and negative going x- and y- directions, the positive z-direction (into the specimen), and the radial distribution function. As an additional useful spatial calculation, we have included the calculation of an "average position vector", which is given by

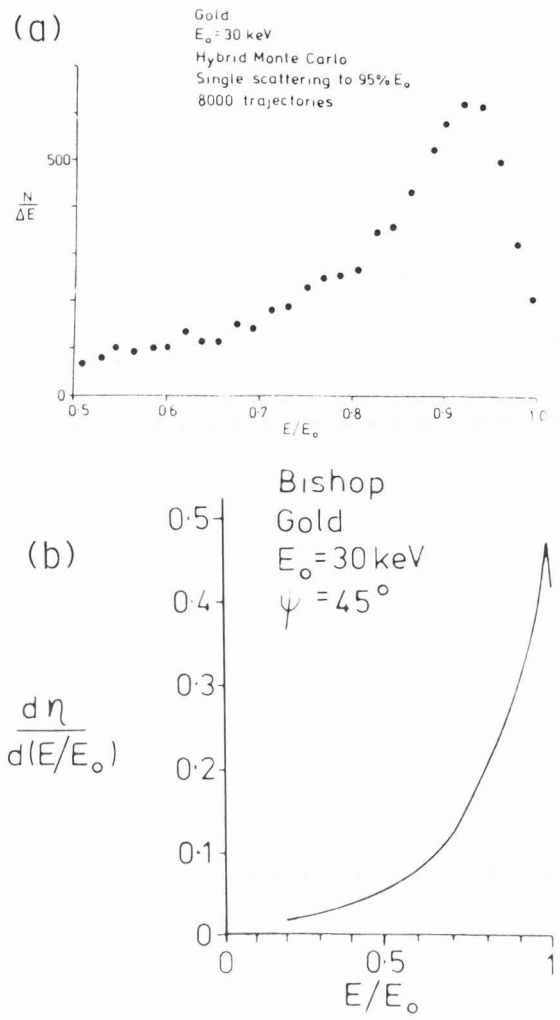


**Fig. 5. (a) Energy distribution of electrons backscattered from a gold target as calculated by Monte Carlo simulation; (b) experimental measurement of energy distribution at a take-off angle of 45° from Bishop (1966).**

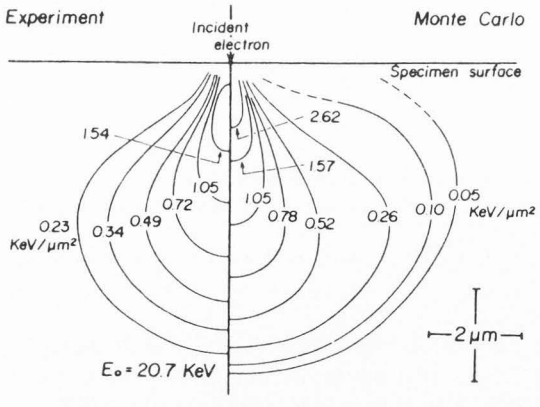


**Fig. 6. Calculation of energy deposition in polymethylmethacrylate and comparison with experiment; from Shimizu et al. (1975).**

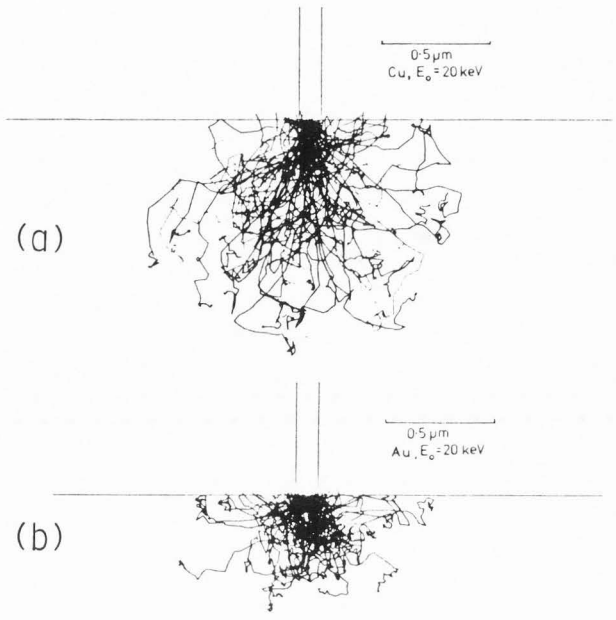


**Fig. 7. Monte Carlo calculations of electron interaction volume in (a) copper and (b) gold at 20 keV; beam size 0.1 micrometer.**

$$X_A = (\sum_i x_i) / N \qquad Y_A = (\sum_i y_i) / N$$

$$Z_A = (\sum_i z_i) / N$$

where i is the index over all scattering events for all trajectories, and N is the total of all scattering events over all trajectories. The value of the average position vector is its immediate utility in confirming that a particular electron beam/specimen configuration has been achieved. Thus, if the electron beam is set normal to the specimen at the origin of coordinates, the symmetry of the beam should yield $X_A = Y_A = 0$ while $Z_A$ has a positive value at approximately 1/3 of the electron range. If the specimen is tilted in a particular calculation, for example about the x-axis, then the symmetry about the origin of coordinates is maintained for the x-axis so that $X_A = 0$, but the interaction volume is now asymmetric along the y-axis so that $Y_A > 0$. The average electron position is especially useful when modifications are made to an existing program. Logic or programming errors which affect the geometry of the electron scattering become immediately apparent in the average position vector if symmetric test conditions are calculated.

### H. X-ray calculations

X-ray calculations can be tested in three main ways: (1) The depth distribution of x-ray production, designated $\phi(\varrho z)$, has been measured experimentally by several authors (Castaing and Henoc, 1966; Brown and Robinson, 1979) for selected systems. Monte Carlo calculations of $\phi(\varrho z)$ curves provide a test of the elastic and inelastic scattering models as well as the energy dependence of the ionization cross section

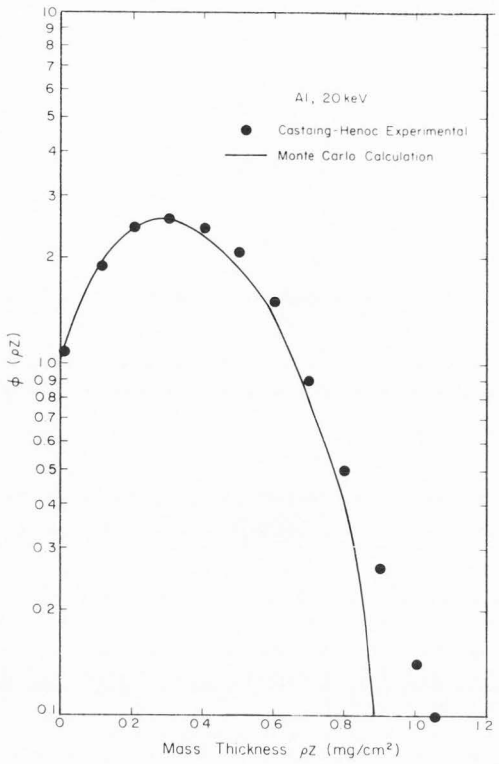


**Fig. 8. Depth distribution of x-ray generation as calculated by Monte Carlo simulation (Myklebust et al. (1976) and as measured experimentally (Castaing and Henoc (1966)). 10000 trajectories were calculated with the Monte Carlo simulation.**

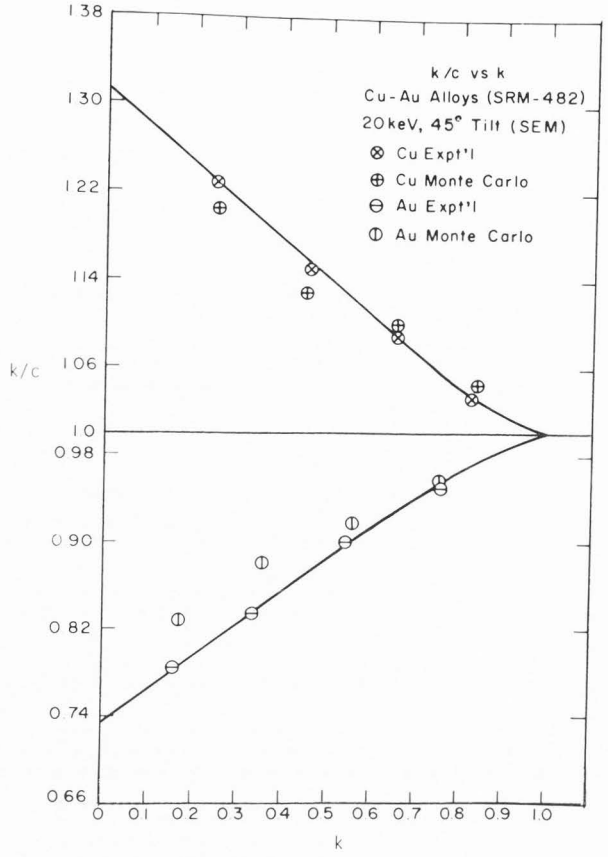


**Fig. 9. Plot of k-value normalized by concentration versus k-value as measured experimentally and calculated with the Monte Carlo simulation (Myklebust et al (1966)).**

which is assumed. An example of such a calculation is shown in Figure 8. Because the distribution is expressed in the terms of a ratio, the $\phi(\varrho z)$ plot is not a good test of the absolute x-ray yield. Moreover, since the energy dependence of most expressions for the cross sections for inner shell ionization is similar, $Q = b \log (cU)/UE_c^2$, where $E_c$ is the critical ionization energy, U is the overvoltage $E/E_c$ where E is the beam energy, and b and c are constants, the $\phi(\varrho z)$ curve does not allow the selection of one cross section in preference to another (Powell, 1976).

(2) The x-ray intensity ratio (k = i(sample)/i(standard)) measured in an electron microprobe from an alloy of known composition can be calculated and compared to the experimental measurement as shown in Figure 9. Again since ratios are calculated, this type of comparison is not sensitive to the exact form of the ionization cross section. Because this type of measurement involves x-rays emitted from the sample, the calculation is sensitive to mass absorption effects. Provided accurate values of the mass absorption coefficients are available, the comparison of k-values directly tests the accuracy of the calculation of the $\phi(\varrho z)$ distribution in the material of the standard and the unknown.

(3) The calculation of absolute x-ray yields and comparison with experiment is not a good test of the Monte Carlo procedure because there is considerable uncertainty in the cross section for inner shell ionization in the continuous overvoltage range from the threshold to approximately five which is employed in the electron microprobe. This fact is demonstrated in Table 3, where calculations for a selection of cross sections for inner shell ionization are compared with experimental results (Newbury and Myklebust, 1979; Lifshin et al., 1977). A substantial range in absolute x-ray yields is noted. Nevertheless, it is still important to make such calculations to determine if the right order of magnitude of the x-ray yield is obtained and if the calculated yields change in the proper way with beam energy.

## Summary

In implementing or changing a Monte Carlo simulation, a logical series of tests should be applied to determine if the calculation produces useful results. One possible sequence of tests to follow is:

(1) Backscatter coefficient as a function of atomic number – adjustments to fitting parameters should be determined at this stage.

(2) Backscatter coefficient as a function of tilt angle.

(3) Backscatter and transmission coefficients of thin foils.

(4) Energy distribution of backscattered electrons.

(5) Spatial distributions, including the average position vector.

(6) X-ray calculations, including $\phi(\varrho z)$, k-values, and absolute x-ray calculations.

**Table 3. Calculation of absolute x-ray yield with various cross sections for inner shell ionization.**

Target: Chromium

| Energy | Green-Cosslett | Fabre | Worthington-Tomlin | Bethe Mott-Massey | Lifshin et al. experiment |
|---|---|---|---|---|---|
| 10 | 2.7E-5 | 2.0E-5 | 1.6E-5 | 6.3E-5 | 4.0E-5 |
| 15 | 9.7E-5 | 8.0E-5 | 5.6E-5 | 1.5E-4 | 1.4E-4 |
| 20 | 1.9E-4 | 1.7E-4 | 1.1E-4 | 2.4E-4 | 2.7E-4 |
| 25 | 2.9E-4 | 2.8E-4 | 1.7E-4 | 3.4E-4 | 4.3E-4 |

all values in photons/electron/steradian

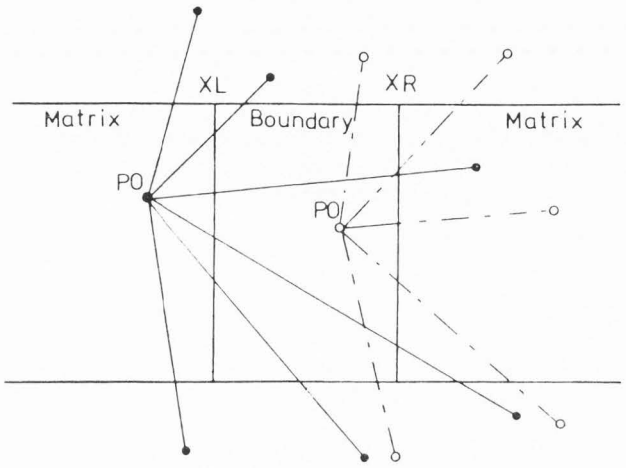


**Fig. 10. Planar boundary slab separating matrix regions. Possible scattering paths from points initially in the matrix (solid lines) and in the boundary (broken lines).**

## SPECIAL GEOMETRIES

A major strength of the Monte Carlo technique is its adaptability to samples with special geometries, e.g., size, shape, internal structure, etc. Since the coordinates of the position of the electron are determined with a step length of the order of the mean free path between scattering points, the electron position can be continuously compared with the function which determines the surface of a target. Conceptually any target which can be described mathematically can be introduced into the Monte Carlo simulation. In reading the literature of the Monte Carlo technique the impression might be obtained that this step is straightforward and trivial. Usually papers describing Monte Carlo simulations do not provide details on the way in which a special target is introduced into the simulation. It is this step which is in fact often the most difficult to implement in a Monte Carlo procedure. As an example of the techniques used to actually introduce a special sample geometry into a calculation, we shall consider in detail the case of a double planar boundary with a variable width, w, oriented perpendicular to the surface of the specimen, as shown in Figure 10. Since the width parameter can be varied, this special geometry can simulate either an interphase boundary between two materials of different composition or it can represent a thin phase at a boundary between two grains of the same composition.

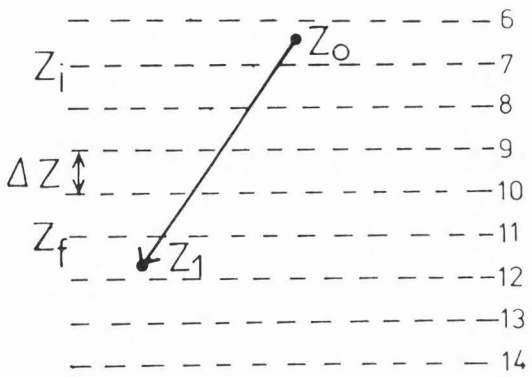


**Fig. 11. Illustration of the technique used to calculate the depth distribution of $\phi(\varrho z)$ histogram.**

### A. Depth distribution of x-ray generation

In particular, we wish to calculate the x-ray production in the two materials of different composition represented by the matrix material "M" and the boundary material "B" in Figure 10. The general concept of the calculation of the depth distribution function $\phi(\varrho z)$ is illustrated in Figure 11, where a portion of the target has been divided into the "boxes" of a histogram. If a scattering step of length S occurs between points with z-coordinates Z0 and Z1, we wish to calculate the contributions of the trajectory element to each box of the histogram. Thus, if $\Delta S$ is the portion of the step length which falls in each box, the x-ray generation to be added to that box in the histogram is given by:

$$\begin{aligned} &\text{IX (x-rays photon/electron)} = Q \text{ (ionizations/e/(atom/cm}^2\text{)} \times N_A \text{ (atoms/mole)} \times (1/A_w) \\ &\text{(moles/g)} \times \varrho \text{(g/cm}^3\text{)} \times \Delta S \text{ (cm)} \times \omega \text{ (x-rays/ionization)} \\ &IX \times Q\, N_A \varrho \omega \Delta S / A_w \end{aligned} \tag{1}$$

where $\omega$ is the fluorescent yield. In some previous Monte Carlo simulations, it was assumed that in calculations for solid targets with relatively coarse $\phi(\varrho z)$ histograms, the x-ray production in a given step could be assigned to the histogram box which contained the initial or final point of the step. While this coarse approximation might be satisfactory for bulk targets of a single composition and with histogram element widths which are significantly greater than the path length of the calculation, it is not satisfactory for the case of the boundary in Figure 10, where electron trajectories will actually cross boundaries between materials of different composition. Moreover, it is not satisfactory for the case of thin foils in the analytical electron microscope to use this coarse approximation, since the mean free path may be approximately equal to thickness and a significant portion of a step may actually lie outside the specimen.

A more complete treatment of the geometry of the step length of the calculation is needed to accurately construct the depth distribution histogram. Considering the situation in

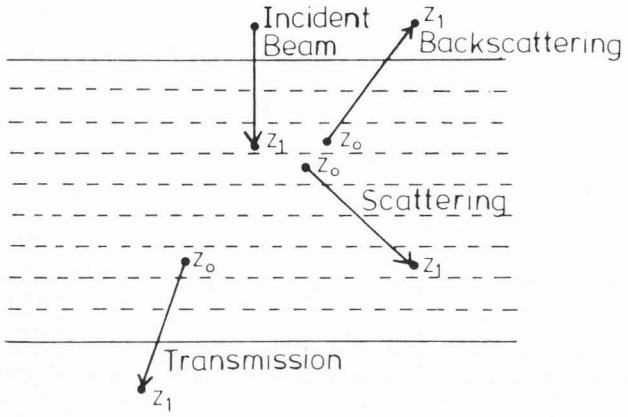


**Fig. 12 Possible scattering paths which must be considered in a complete calculation of the depth distribution histogram.**

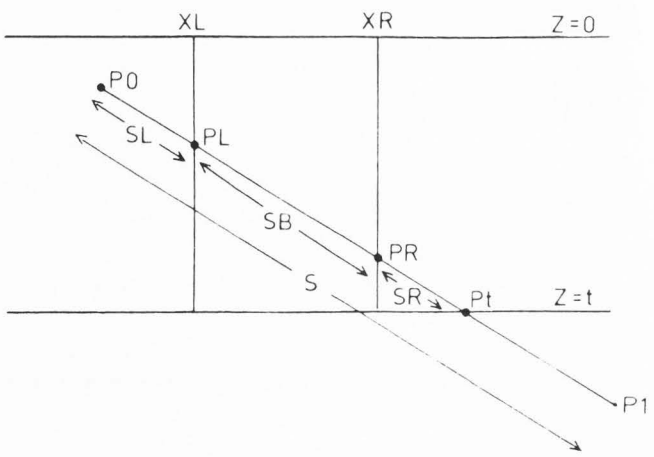


**Fig. 13. Detailed analysis of step segments which must be considered in a complete calculation of the depth distribution histogram.**

Figure 11, the calculation can be divided into three sections: (1) the initial incomplete box; (2) the central complete boxes; and (3) the final incomplete box. Considering the complete boxes, for a trajectory step length S which occurs at an arbitrary angle $\epsilon$ from the normal,

$$\cos \epsilon = (Z1 - Z0)/S \text{ and } \cos \epsilon = \Delta Z/\Delta Sc$$

where Z is the width of the histogram boxes. From these equations

$$\Delta Sc = \Delta Z S/ \mid (Z1 - Z0) \mid \quad (2)$$

Thus, the x-ray contributions to the complete boxes in the histogram are given by the equation (1) with $\Delta S = \Delta Sc$.

For the initial incomplete box, the relation becomes $\cos \epsilon = (Zi - Z0)/\Delta Si$ so that

$$\Delta Si = (Zi - Z0)\, S/(Z1 - Z0) \quad (3)$$

where Zi represents the Z-value of the bottom of the histogram box.

For the final incomplete box, the relation is $\cos \epsilon = (Z1 - Zf)/\Delta SE$ which gives

$$\Delta Sf = (Z1 - Zf)\, S/(Z1 - Z0) \quad (4)$$

In addition to the general case of Figure 11, three special cases must be considered, Figure 12: (1) incident beam — The incident beam penetrates through the surface at $Z0 = 0$, so that equation (3) becomes:

$$\Delta Si - Zi\, S/Z1 \quad (5)$$

(2) Backscattering: In this case part of the step S lies outside of the target. It is necessary to calculate the portion of the step S′ which lies within the target. This portion is found by taking

$$S' = ABS\,[(Z0 - ZS)/C] \quad (6)$$

where ABS is the absolute value of the function, C is the direction cosine of the trajectory step S, and ZS is the z-coordinate of the surface; for a flat specimen $ZS = 0$. S′ is substituted for S in equations (2)-(4).

(3) Transmission: Again an incomplete step must be calculated. In this case the electron penetrates the bottom of the foil so that it escapes at $Z = Zt$. The portion of the step within the specimen is given by

$$S' = ABS\,[(Zt - Z0)/C] \quad (7)$$

This partial step length is again used in equations (2)-(4).

### B. Boundary Case

Having considered the division of the trajectory step in a single phase sample to obtain the depth distribution function, the situation of the planar boundary can now be considered. The possible cases are illustrated in Figure 10. The electron may cross one or more boundaries and may exit the specimen either by backscattering, or alternatively, if the specimen is in the form of a thin foil, transmission may occur. In order to calculate the depth distribution function separately for the matrix and grain boundary phases, the portions of the step lengths in each phase must be calculated, correcting for any path length outside the specimen. The sequence of steps for this type of calculation will be illustrated for the path shown in Figure 13. This path originates in the left matrix with average atomic number Zm, penetrates the boundary where the average atomic number for the boundary material is Zb, passes through the right matrix, and transmits through the sample.

**Step 1.** The initial point (X0, Y0, Z0), the step length S, and the tentative final point (X1, Y1, Z1) are known initially, as well as the direction cosines of the segment, A, B, C. The portion of the step within the left matrix is calculated. Since this portion of the step terminates on the left edge of the boundary where X = XL, the length of the path within the left matrix is given by

$$SL = (XL - X0)/A \quad (8a)$$

The y- and z- coordinates of the boundary intersection are then

$$YL = Y0 + SL \times B \quad (8b)$$
$$ZL = Z0 + SL \times C \quad (8c)$$

This step length SL and the initial (X0, Y0, Z0) and final (XL, YL, ZL) points can now be substituted in equations (1)-(4) to calculate the contributions to the matrix histogram.

**Step 2.** Segment in structure. Initially we know that the electron has crossed the structure entirely. The length of this segment must then be

$$SB = (XR - XL)/A \quad (9a)$$

Because the boundary material can have a different average atomic number than the matrix, the elastic scattering probability will be different, and the step length must be adjusted for this effect. Since the screened Rutherford elastic scattering cross section is proportional to the 4/3 power of the average atomic number:

$$SB' = SB\,ZM^{4/3}/Zb^{4/3} \quad (9b)$$

The modified step segment within the boundary material may be longer or shorter than before. The portion of the step in the right matrix SR is calculated from:

$$SR = S - SL - SB' \quad (9c)$$

**Step 3.** If SR is negative, this implies that the step segment within the boundary material has shortened sufficiently to pull the endpoint back within the boundary. If this is the case, then

$$X1 = XL + SB' \times A \quad (9d)$$
$$Y1 = YL + SB' \times B \quad (9e)$$
$$Z1 = ZL + SB' \times C \quad (9f)$$

The depth distribution histogram contributions for the boundary region are now calculated with the step segment length SB′ and endpoints (XL, YL, ZL) and (X1, Y1, Z1) in equations (1)-(4). The calculation is now complete and the next scattering act starts at (X1, Y1, Z1) in the boundary material.

**Step 4.** If SR is positive, then the full value of SB from equation (9a) must be used to calculate the endpoint on the right boundary:

$$XR = XR \quad (9g)$$
$$YR = YL + SB \times B \quad (9h)$$
$$ZR = ZL + SB \times C \quad (9i)$$

The depth distribution histogram for the boundary is calculated with the step segment SB and the endpoints (XL, YL, ZL) and (XR, YR, ZR) in equations (1)-(4).

**Step 5.** If SR is positive, then some portion of the step has penetrated the right matrix. This step segment SR has a new value

$$SR' = SB' - SB + SR \quad (9j)$$

which reflects the modification to the scattering caused by traversing the boundary material. The final point in the right hand matrix is calculated:

$$X1 = XR + SR' \times A \quad (9k)$$
$$Y1 = YR + SR' \times B \quad (9l)$$
$$Z1 = ZR + SR' \times C \quad (9m)$$

Z1 is checked to determine if it is within the foil. If it is, then the depth distribution histogram for the matrix is calculated with the step segment SR′ and the endpoints (XR, YR, ZR) and (X1, Y1, Z1). If transmission has occurred, then the portion of SR″ within the foil is calculated:

$$SR'' = (Zt - ZR)/C \quad (9n)$$

The exit coordinates are:

$$Z = Zt \quad (9o)$$
$$X = XR + SR'' \times A \quad (9p)$$
$$Y = YR + SR'' \times B \quad (9q)$$

These arguments can be extended to the other paths shown in Figure 10 to fully characterize all possible cases involving the boundary.

This procedure has been recently applied to the calculation of interactions of electrons in real structures containing interphase boundaries:

**Table 4. Intensity profile across an $\alpha$ / $\gamma$ interface in U-Nb**

Thickness: 110 nm; Energy: 100 keV; Beam diameter: 18 nm
Ratio = Nb (position) / (pure phase)

Source: Romig et al. (1982)

| Position, nm | Measured Ratio | Calculated Ratio |
|---|---|---|
| −100 | 1.0 | .98 |
| −90 | 1.0 | .98 |
| −80 | .98 | .97 |
| −70 | .99 | .98 |
| −60 | .99 | .96 |
| −50 | .98 | .96 |
| −40 | .95 | .96 |
| −30 | .93 | .94 |
| −20 | .91 | .91 |
| −20 | .84 | .83 |
| 0 | .51 | .51 |
| 10 | .20 | .19 |
| 20 | .13 | .10 |
| 30 | .091 | .070 |
| 40 | .066 | .054 |
| 50 | .052 | .044 |
| 60 | .041 | .037 |
| 70 | .018 | .028 |
| 80 | .006 | .029 |
| 90 | 0.0 | .026 |
| 100 | 0.0 | .023 |

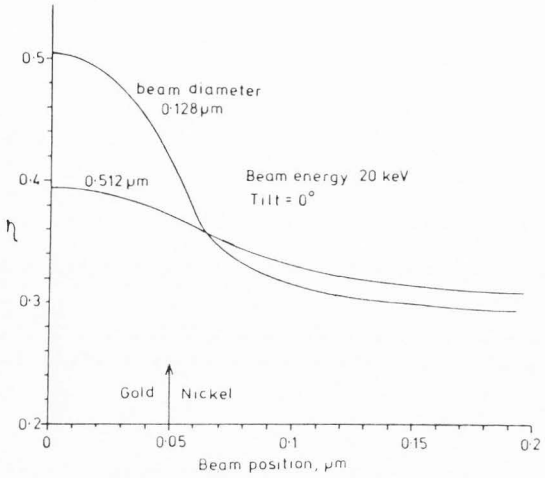


**Fig. 14. Total electron backscatter coefficient calculated when a beam is scanned across a gold slab 0.1 micrometer wide in a bulk nickel matrix. 10,000 trajectories were calculated at each point in the profile.**

(1) Thin foil: Romig et al (1982) have calculated and measured intensity profiles across interphase boundaries involving alpha-uranium and a second phase which contains uranium and solute element, niobium or molybdenum, with the solute element located exclusively in the second phase. An example of the profile of the intensity ratio I(Nb)/I(Nb, second phase) for a foil 110 nm thick at a beam energy of 100 keV is given in Table 4. Good correspondence is found, especially in the immediate region of the boundary where the signals are changing rapidly.

(2) Thick specimen: Newbury, Myklebust, and Kyser (unpublished results) have calculated the response of the total backscattered electron and characteristic x-ray signals as a beam is moved across an 0.1 micrometer wide gold slab set in a nickel matrix (NBS Standard Reference Material 484, magnification standard). The backscattered electron signal as a function of position is shown in Figure 14 for the beam sizes. Experimental profiles are currently being collected for comparison with these calculated profiles.

The value of the Monte Carlo calculations in both of these examples is the potential utility in deconvoluting measured signal profiles for beam scattering effects to yield information about the true structure of the sample, which is otherwise distorted by electron scattering effects.

## Summary

Application of the Monte Carlo simulation to even a simple planar boundary requires careful consideration of the exact nature of the structure. A stepwise approach is necessary in which each segment of the trajectory is calculated sequentially to find the proper segments in each material. Each new structure shape requires special consideration of its particular geometery. When this is done, the resulting simulation provides a powerful tool for exploring the signals.

## REFERENCES

Bishop H. (1966). Some Electron Backscattering Measurements for Solid Targets, in: X-ray Optics and Microanalysis, R. Castaing, P. Deschamps, and J. Philibert (eds.), Hermann, Paris, 153-158.

Brown JD, Robinson WH. (1979). Quantitative Analysis by $\phi(\rho z)$ Curves, in: Microbeam Analysis—1979, D.E. Newbury (ed.), San Francisco Press, 238-240.

Castaing R, Henoc J. (1966). Repartition en profondeur du rayonnement characteristique, in: X-ray Optics and Microanalysis, op. cit., 120-128.

Cosslett VE, Thomas RN. (1964). Multiple Scattering of 5-30 keV Electrons in Evaporated Metal Films I: Total Transmission and Angular Distribution. Brit. J.A.P. **15**, 883-907.

Curgenven L, Duncumb P. (1971). Simulation of Electron Trajectories by a Simple Monte Carlo Technique, in: Tube Investments Res. Lab Report 303, Tube Investments, Hinxton Hall, Saffron Walden, Essex, England.

Heinrich KFJ. (1966). Electron Probe Microanalysis by Specimen Current Measurement, in: X-ray Optics and Microanalysis, op. cit., 159-167.

Heinrich KFJ, Newbury DE, Yakowitz H. (1976). Use of Monte Carlo Calculations in Electron Probe Microanalysis and Scanning Electron Microscopy. National Bureau of Standards Special Publication 460, Washington, DC 20234.

Kyser DF. (1981). Monte Carlo Calculations for Electron Microscopy, Microanalysis, and Microlithography. Scanning Electron Microsc. 1981; I:47-62.

Kyser DF, Murata K. (1974). Quantitative Electron Microprobe Analysis of Thin Films on Substrates. IBM J. Res. Dev. **18**, 352-363.

Lifshin E, Ciccarelli MF, Bolon RB. (1977). New Measurements of the Voltage Dependence of Absolute X-ray Yields using Energy Dispersive X-ray Spectrometry, in: 12th Ann. Conf. Microbeam Analysis Society, RE Ogilvie (ed.), San Francisco Press, 104A-104C.

Myklebust RL, Newbury DE, Yakowitz H. (1976). NBS Monte Carlo Electron Trajectory Calculation Program, in: NBS SP 460, op cit., 105-128.

Newbury DE, Myklebust RL. (1979). Monte Carlo Calculations of Absolute X-ray Generation from Solid Targets, in: Microbeam Analysis—1979, op. cit., 51-53.

Newbury DE, Myklebust RL. (1981). A Monte Carlo Electron Trajectory Simulation for Analytical Electron Microscopy, in: Analytical Electron Microscopy—1981, R. Geiss (ed.), San Francisco Press, 91-98.

Powel CJ. (1976). Evaluation of Formulas for Inner Shell Ionization Cross Sections, in: NBS SP 460, op cit., 97-104.

Reimer L, Krefting ER. (1976). The Effect of Scattering Models on the Results of Monte Carlo Calculations, in: NBS SP 460, op. cit., 45-60.

Romig AD Jr., Newbury DE, Myklebust RL. (1982). Beam Broadening in a Strongly Scattering Target in the Analytical Electron Microscope, in: Microbeam Analysis – 1982, K.F.J. Heinrich (ed.), San Francisco Press, 88-92.

Shimizu R, Murata K. (1971). Monte Carlo Calculations of Electron-Sample Interactions in the SEM. J.A.P., **42**, 387-394.

Shimizu R, Ikuta T, Everhart TE, DeVore WJ. (1975). Experimental and Theoretical Study of Energy Dissipation Profiles of keV Electrons in Polymethylmethacrylate. J.A.P., 1581-1584.

Wells OC. (1975). Measurements of Low-loss Electron Emission from Amorphous Targets, Scanning Electron Microsc. 1975, 43-50.